

Electronic States in One, Two, and Three Dimensional Highly Amorphous Materials: A Tight Binding Treatment

D. J. Priour, Jr¹

¹*Department of Physics, University of Missouri, Kansas City, Missouri 64110, USA*

(Dated: July 28, 2021)

In a tight binding framework, we analyze the characteristics of electronic states in strongly disordered materials (hopping sites are placed randomly with no local order) with tunneling matrix elements decaying exponentially in the atomic separation with various decay ranges l examined. We calculate the density of states (DOS) and the Inverse Participation Ratio (IPR) for amorphous atomic configurations in one, two, and three dimensions. With a finite size scaling analysis of the IPR statistical distributions, it is shown that states are either extended or localized for a particular energy, and phase portraits for wave functions are obtained showing extended and localized behavior in the thermodynamic limit. While we conclude that all states are localized in 1D, in the 2D case there is a threshold for l above which some eigenstates appear to be extended and below which wave functions are entirely localized. For 3D geometries, there are two mobility boundaries flanking an intermediate range of energies where states are extended with eigenstates localized for energies above or below this range. While a zone of extended states persists even for very short l , the width of the region tends to zero exponentially (i.e. scaling as $e^{-A/l}$) for very small decay length scales.

PACS numbers: 72.15.Rn, 72.80.Ng, 71.23.-k, 71.23.An

I. INTRODUCTION AND THEORETICAL FRAMEWORK

A periodic crystal in the absence of disorder supports extended Bloch waves within the bounds of energy bands¹. However, the nature of the electronic states in a strongly disordered (i.e. amorphous) material where symmetry with respect to discrete translations is absent, is a more subtle question. Our aim is to examine the effect of very strong disorder on transport characteristics.

Operating in the framework of a tight binding model where electrons are localized in atomic sites or dopant impurities, we examine amorphous materials in one, two, and three dimensions where the locations of atoms are taken to be uncorrelated and randomly distributed within the medium. Atomic or dopant configurations with no local ordering of the sites are described as gas-like disorder² with relevance to the transport characteristics associated with expanded alkali metals³ as well as impurity bands in silicon. The characteristics of exciton states with respect to localization have been examined in the context of similar types of disorder⁴. In broader generality, formal analytical and computer studies have calculated the Density of States in amorphous materials with no correlations among the site positions⁵⁻⁸.

Disorder, even in regular lattices, may be manifest as random site energies which can disrupt the extended character of itinerant states and thereby create conditions for localization. Our aim is to examine strongly disordered materials and the properties of the associated electronic states with respect to localization. However, we do not introduce a random site energy, and in this sense our work is complementary to studies where random potentials are superimposed on sites in a periodic crystalline geometry⁹⁻¹³. Instead of examining a system on a regular lattice geometry, we calculate electronic

wave functions for the fully amorphous case and examine how strong positional disorder, in conjunction with tunneling matrix elements which decay exponentially in the separation of neighboring hopping sites, affects the characteristics of eigenstates with respect to localization.

Off-diagonal disorder which enters in random variations in tunneling matrix elements controlling hopping among sites in the absence of a random on-site potential, has been of interest since an early study by F. J. Dyson¹⁴⁻²⁰. Calculations related to the density of states⁶⁻⁸ and aspects of localization^{4,5,21} have been carried out in the context of a 3D gas-like tight binding model. We report on results relevant to the aim of finding out by direct calculation in a large-scale statistical study the extent to which wave functions are localized in amorphous materials and under what conditions eigenstates are extended. Moreover, we obtain phase portraits showing for different energies and ranges l of the hopping integral domains of extended and localized states.

In this work, we use for the tight binding Hamiltonian

$$\mathcal{H} = -\frac{1}{2}t_0 \sum_{i=1}^N \sum_{j \neq i} V(r_{ij})(\hat{c}_i^\dagger \hat{c}_j + \hat{c}_i \hat{c}_j^\dagger) \quad (1)$$

where the sum over the index “ i ” ranges over the N particles contained in the simulation volume, we take the hopping parameter t_0 to be 3.0 electron volts, and the factor of “ $1/2$ ” compensates for multiple counting of the hopping terms between atoms. The creation and destruction operators \hat{c}^\dagger and \hat{c} create and destroy occupied electronic orbitals at sites indicated by the subscript. For the hopping integral, we use $V(r_{ij}) = e^{-\gamma r_{ij}/s}$, where r_{ij} is the separation between sites i and j , $s = \rho^{-1/D}$ is the typical inter-orbital separation, ρ is the volume density of sites, D is the dimensionality of the system, and γ is a dimensionless parameter. With the hopping integrals expressed

in this manner and the length scale for the decay of the hopping matrix element thus being $l = s/\gamma$, large/small γ values correspond to decay lengths small/large in relation to the typical interatomic separation. For the sake of convenience, we rescale coordinates such that $\rho = 1$, with a simple inverse relationship $l = \gamma^{-1}$ among the hopping length scale l and decay parameter γ and $V(r_{ij}) = e^{-\gamma r_{ij}}$ for the dependence of the tunneling matrix element. Although the hopping integral $V(r_{ij})$ is finite in range by virtue of the exponential decay, we nevertheless take into consideration hopping among all pairs of orbitals contained in the system of N sites with only a negligible increase (i.e. a contribution on the order of N^2) where direct diagonalization, which scales as N^3 and constitutes the main computational bottleneck, is used to calculate the electronic states.

Our Hamiltonian does not incorporate perturbations of the on-site energy term (for convenience all site energies are set to zero), and disorder instead enters in the off-diagonal tunneling matrix elements. Thus, our program in this work is to investigate the effect of positional disorder itself on transport characteristics. Although the treatment is nonperturbative with no local order in the locations of the sites in the amorphous systems we examine, the decay length scale l of the hopping integral serves to parameterize the disorder strength. For large l (small γ), the tunneling is long-ranged and connects sites to many neighbors, effectively averaging over the hopping rates to and from many orbitals and thereby somewhat muting the effect of positional disorder. On the other hand, if l is small relative to the typical inter-site spacing $\rho^{-1/D}$ (i.e. for large γ), the tunneling is preponderantly to the very closest neighbors; moreover, even small fluctuations in the locations of nearest neighbors impact charge transport through the site to a significant degree via the exponential dependence of the hopping integral. Hence, disorder is in a sense amplified as γ is increased and muted when γ is small.

In calculating the tight binding wave functions, we examine a L^D supercell, where many system sizes are considered in order to perform finite size scaling and determine the degree to which eigenstates are localized in the bulk limit. Energies obtained by diagonalizing the tight binding (Hermitian) Hamiltonian are used to construct the global density of states (DOS), while the eigenstates themselves are retained for analysis to characterize the electronic wave functions with respect to localization with the aid of a single quantity known as the

Inverse Participation Ratio (IPR), $\sum_{i=1}^N |\psi_i|^4 / (\sum_{i=1}^N |\psi_i|^2)^2$.

The participation ratio shows distinct behavior depending on whether the wave function is confined to a small volume or spread out over a larger region, and hence more extended in character. While in the former case the IPR is finite and tends to be relatively large, the participation ratio is smaller for broader electronic states, and approaches zero as the wave function becomes spread

over a bulk system in the case of a genuinely extended state. This dichotomy for extended *vis à vis* localized states makes the IPR a useful diagnostic parameter in the context of theoretical calculations where often the participation ratio provides information as to the extent of localization of carrier wave functions in specific locations in an amorphous geometry or in certain energy ranges of a band structure²²⁻²⁶.

In this work, we aim to determine for very large 1D, 2D, and 3D amorphous systems the prevalence of extended states, and we construct phase portraits showing where wave functions are localized and where states are extended. The random character of the disorder precludes a direct observation of the evolution of the characteristics of electronic states as the system size L is increased. However, there remains the possibility of determining in a statistical sense the localization characteristics of the amorphous medium by calculating the Inverse Participation Ratio histogram. Shifts in the weight of the IPR probability distribution with increasing L provide information as to how many of the electronic states ultimately are localized and what portion are genuinely extended. For a specific hopping integral decay parameter γ we find the status of electronic states with respect to localization to be determined exclusively by the energy eigenvalue, with no situation arising in which localized and extended states exist simultaneously for the same infinitesimal energy interval. With a finite size scaling analysis of the Participation ratio histogram calculated for various system sizes, we extrapolate to the bulk limit and determine in a rigorous fashion energies where electronic states are localized, and eigenenergies supporting extended states.

By repeating the calculation for different γ , we obtain phase portraits showing regions of localized and extended wave functions. The IPR probability distributions represent an intermediate stage in the determination of energy ranges corresponding to localized or extended states in the bulk limit, but are of interest in themselves and highlight salient qualitative trends. A participation ratio histogram which does not change either in its shape or position with increasing system size signifies that all states encompassed in the distribution are localized, and the IPR distribution may be regarded as a bulk characteristic where $L \gg \xi$ with ξ being the localization length scale of the eigenstates. At the opposite extreme is a Participation ratio histogram which shifts in its entirety toward smaller IPR values with increasing L . The steady transfer of a large share of statistical weight toward even smaller participation ratios implies the electronic states are preponderantly extended. A possibility interpolating between the two extremes arises if a part of the IPR distribution converges as would be expected for a set of localized states while at the same time a portion of the histogram separates from the main envelope of the distribution and is conveyed toward lower IPR values.

To sample realizations of disorder from the appropriate statistical distribution, it is important to generate

random configurations of atoms in an unbiased way. For stochastic input, we use a Mersenne Twister algorithm to minimize correlations among successively generated random numbers and to ensure the period of the pseudorandom sequence far exceeds the quantity of random numbers used over the course of the simulations. For continuously distributed hopping sites, the number N of sites in the simulation volume must in general vary from one sample to the next due to statistical fluctuations. The integer value closest to the mean occupancy $N_{\text{av}} = \rho L^D$ is a convenient initial choice, and random variations in the number of particles in the simulation volume are taken into account with a sequence of stochastically driven attempts either to raise or lower N . The latter are part of an importance sampling scheme similar to that used to derive the Metropolis Criterion²⁸ at the heart of Monte Carlo simulations which sample the Boltzmann distribution in the calculation of thermodynamic variables.

To determine the probability of N sites in $v = L^D$, we divide v into M sub-volumes of equal size where $\Delta v = v/M$. For large M the likelihood of multiple occupancy in any of the sub-volumes is very small relative to the chance of having one or zero sites in a subdivision; in the small Δv limit, the single occupancy probability is $\rho \Delta v$, with $(1 - \rho \Delta v)$ being the complementary likelihood of null occupancy. Hence, the probability the entire system is devoid of hopping sites is $(1 - \rho v/M)^M$, which becomes $e^{-\rho v}$ for $M \rightarrow \infty$. For single occupancy, adopting a prefactor M to take into consideration that the site may reside in any of the M sub-volumes, yields $M(\rho v/M)(1 - \rho v/M)^{M-1}$, which becomes $\rho v e^{-\rho v}$ in the $\delta v \rightarrow 0$ limit. Similar logic is used for general case, and the probability for having exactly N sites in the simulation volume is $P(N) = e^{-\rho v} (\rho v)^N / N!$ where $N!$ is a combinatorial factor to compensate for multiple counting.

To generate a realization of disorder, a succession of attempts (a number of moves in the vicinity of N_{av} is sufficient to achieve ergodicity) is made to raise or lower the occupancy number N , where the choice to increase or decrease N is randomly determined. For increments from N to $N + 1$, the relevant criterion is the probability ratio $r_+ \equiv p(N + 1)/p(N) = \rho v/(N + 1)$, and the change is accepted if $X_r < r_+$, where X_r is a random number sampled uniformly from the interval $[0, 1]$. Similarly, decreasing N to $N - 1$ occurs if $X_r < r_-$ where $r_- = p(N - 1)/p(N) = N/\rho v$. With N properly sampled, D Cartesian coordinates for each site location are chosen independently (and at random with uniform probability density) from the interval $[0, L]$.

The coordinates for each of the N sites enter in the construction of the Hamiltonian matrix (in the context of the tight binding model given in Eq. 1), which is diagonalized for the eigenenergies and eigenstates; periodic boundary conditions are implemented to mitigate finite size effects. For the purpose of the DOS calculations, 5×10^5 energy eigenvalues are sampled; in obtaining the IPR statistical distributions, where eigenstates are used

to calculate participation ratios with a concomitant increase in the computational burden, 10^5 wave functions are retained.

In each section of this work, we present and discuss results for 1D, 2D, and 3D systems; for each dimensionality, we examine a range of tunneling matrix element decay parameters γ which in a sense govern the strength of the disorder. In Section II, we examine the Density of States for energy eigenvalues. Inverse Participation Ratio (IPR) statistical distributions are discussed in Section III with IPR histograms displayed for various system sizes. In Section IV, the channel averaged participation ratios are shown; we argue that IPR channel averages are representative of a particular energy and hence may be used to determine how the IPR scales with system size. Ultimately, in Section V, a finite size scaling analysis of the participation ratio channel averages is used to extrapolate to the thermodynamic limit and thereby yield the mean bulk IPR. The latter, used to construct phase portraits showing where states are extended or localized for different values of E and γ , indicates for $D = 3$ a zone of extended states in the midst of a region of localized states and flanked by two mobility boundaries. Although a finite fraction of the states are extended even for large γ where disorder fluctuations are very important, the width of the interval of energies $w(\gamma)$ where states are extended decreases rapidly for large to moderate γ , with an asymptotically exponential dependence $w(\gamma) \sim e^{-A\gamma}$. Conclusions are presented in Section VI.

II. ENERGY DENSITY OF STATES

The DOS, which in principal is a continuous function $f(E)$ of energy for an amorphous material, may only be rendered to an approximate degree in a finite calculation. Accordingly, we partition the energy interval between the ground state and the uppermost excited state into a finite though reasonably large number of sub-intervals or “bins”. The augmented resolution achieved with an increase in the total number of partitions is counterbalanced with a rise in the magnitude of statistical fluctuations. To strike a suitable balance among detail and noise, 500 divisions are used in preparing DOS histograms; with a total of 5×10^5 eigenvalues for each DOS curve, choosing 500 bins still allows on average for 1,000 data point for each partition.

We examine DOS curves for 1D, 2D, and 3D systems, for which a salient common characteristic is a rapid convergence of the energy eigenvalue statistical distributions with respect to the system size L . In fact, as may be seen for representative cases in Fig. 1, the DOS curves overlap very closely and approach the bulk limit as long as $L \gg \max[\rho^{-1/D}, l]$ with the hopping range l and the typical interparticle separation $\rho^{-1/D}$ (unity in our treatment) being relevant length scales.

Another important trend seen for all dimensionalities under consideration is a systematic shift of the DOS sta-

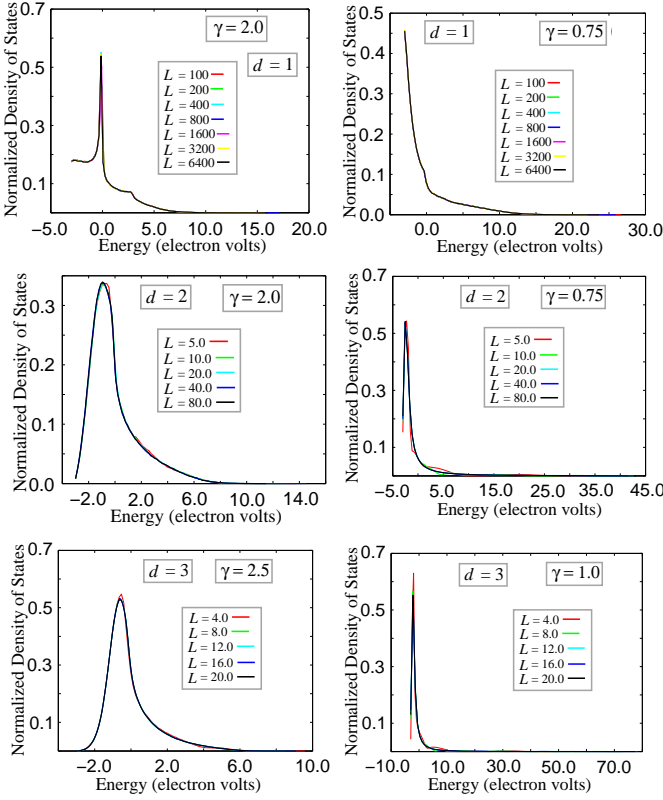


FIG. 1: (Color Online) Density of states plotted for (top to bottom) $D = 1$, $D = 2$, and $D = 3$, and for large to small γ (left to right). DOS curves are plotted for various systems sizes L .

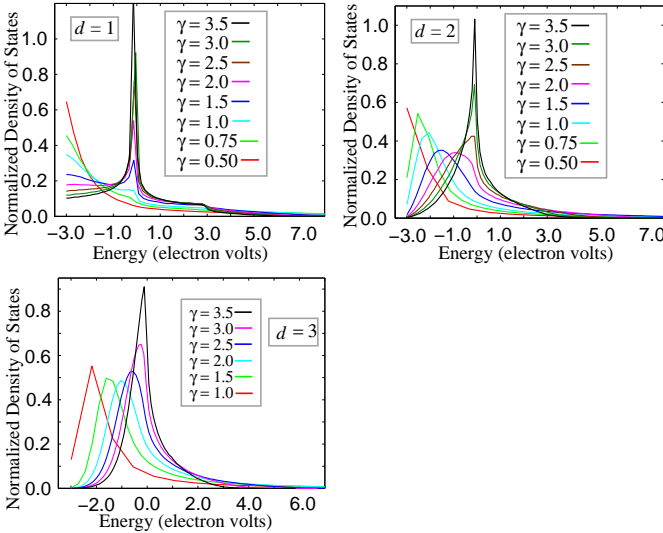


FIG. 2: (Color Online) Density of States curves are shown together for a range of decay rates γ , with, clockwise from left, $D = 1$, $D = 2$, and $D = 3$.

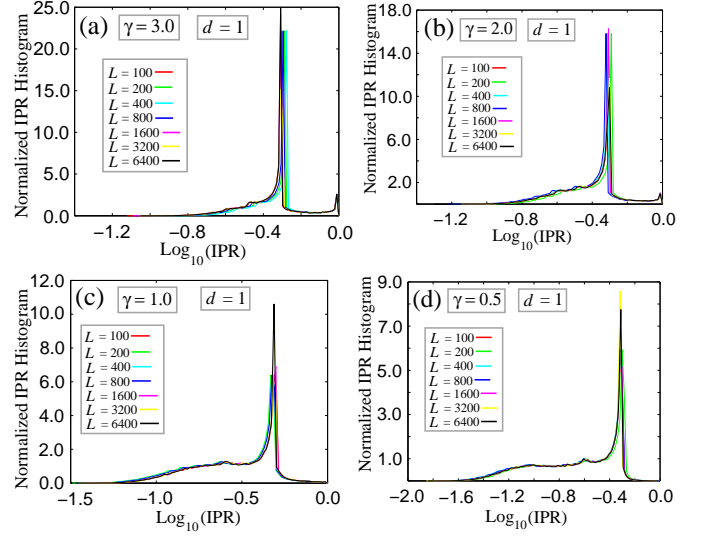


FIG. 3: (Color Online) Inverse Participation Ratio profiles graphed for various system sizes L for hopping integral decay rates ranging from $\gamma = 3.0$ in panel (a) to $\gamma = 0.5$ in panel (d) for 1D systems.

tistical weight toward lower (i.e. more negative) energies with decreasing γ , or increasing tunneling matrix element range $l = \gamma^{-1}$ shown. In Fig. 2 DOS curves are displayed for $D = \{1, 2, 3\}$ for a broad range of γ values with results (calculated for large L) converged with respect to the size of the system.

Although a shift of statistical weight toward negative energy values occurs for each dimensionality, the evolution of the DOS curves for 1D systems differs from that seen for $D = 2$ and $D = 3$. For $D = 1$, the energy probability distribution has a single maximum centered about $E = 0$ for $\gamma \gg 1$. However, with increasing $l = \gamma^{-1}$, a secondary peak appears at a negative energy, gaining amplitude at the expense of the probability density near the $E = 0$ maximum; for large enough l , the latter vanishes with only the negative energy peak remaining.

For two and three dimensional systems, probability density is transferred from $E = 0$ to negative energies as in the case $D = 1$. However, instead of an intermediate transition to a dual peak profile, the DOS curves remain unimodal as the single maximum migrates continuously toward lower energies, arriving at a negative energy for $\gamma \ll 1$.

III. PARTICIPATION RATIO STATISTICAL DISTRIBUTIONS

The Inverse Participation Ratio (IPR) is a compact single parameter gauging the degree to which electronic states are localized or extended, with the IPR tending to zero for $L \rightarrow \infty$ for bulk extended states. While our aim in this work is to extrapolate to the bulk limit in a quantitative fashion, information may also be gleaned

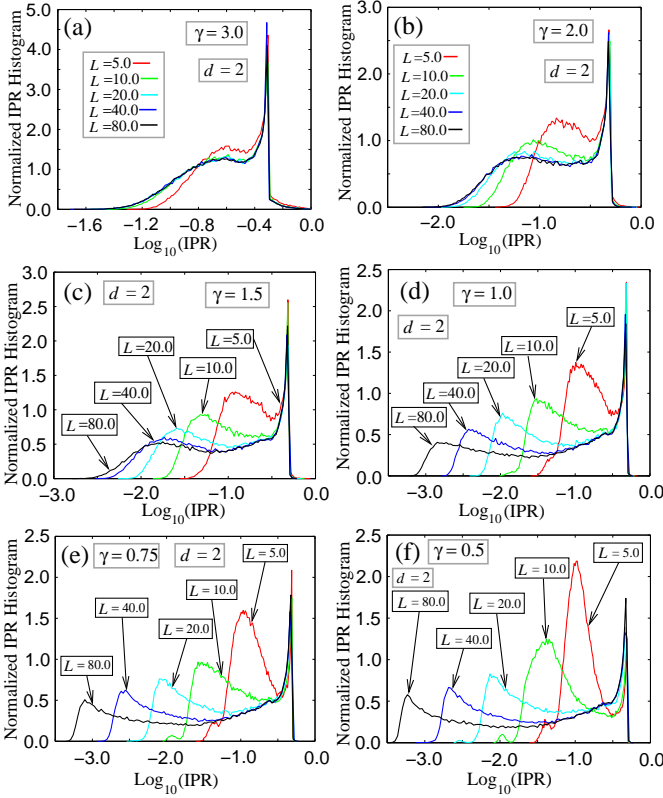


FIG. 4: (Color Online) Inverse Participation Ratio profiles graphed for various system sizes L for hopping integral decay rates ranging from $\gamma = 3.0$ in panel (a) to $\gamma = 0.5$ in panel (f) for 2D systems.

at a qualitative level when participation ratio curves are juxtaposed for a range of system sizes. Since the IPR may vary by several orders of magnitude over the full gamut of system sizes L under consideration, it is often more prudent to exhibit $\log_{10}(\text{IPR})$ in lieu of the raw participation ratios.

The IPR histograms are created by dividing the interval along the $\log_{10}(\text{IPR})$ abscissa into a suitable number of bins. With the availability of 10^5 participation ratios, the choice of 200 partitions provides a reasonable measure of resolution while keeping statistical fluctuations at reasonable levels. IPR distributions are shown in Fig. 3, Fig. 4, and Fig. 5 for $D = 1$, $D = 2$, and $D = 3$ respectively.

In the 1D case, the system sizes progress geometrically, doubling from $L = 100$ to $L = 6400$. With successive doublings of L , the IPR histograms invariably converge and cease to evolve with increases in the system size, a characteristic consistent with the localization of all wave functions in the thermodynamic limit. When converged in L to an IPR distribution appropriate to the bulk limit, histograms are dominated by cusp-like peaks near the upper limit of the IPR range. The latter characteristic is a hallmark particular to 1D systems and is evident whether the hopping integral length scale l is large or

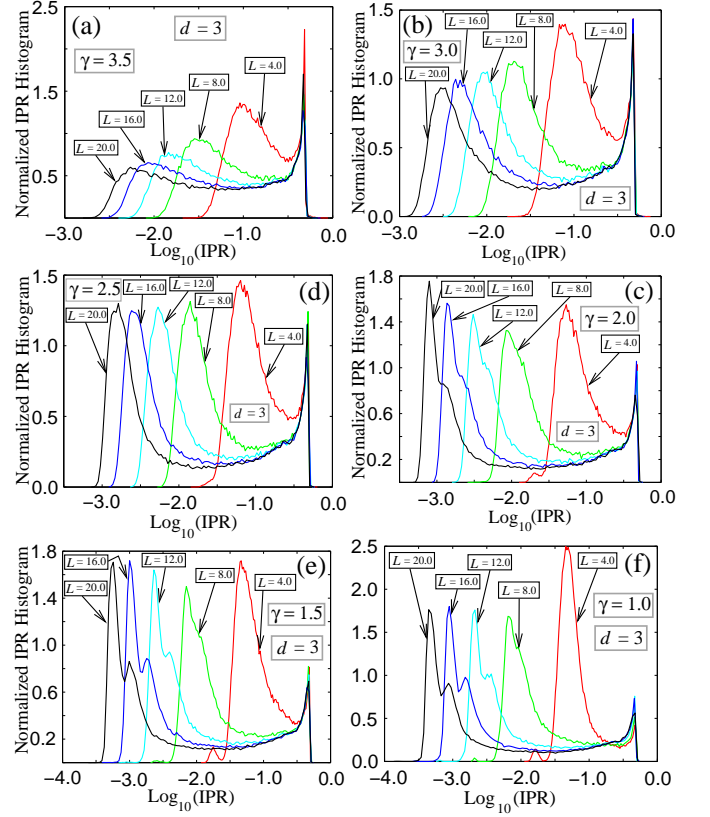


FIG. 5: (Color Online) Inverse Participation Ratio profiles graphed for various system size L for hopping integral decay rates γ ranging from $\gamma = 3.5$ in panel (a) to $\gamma = 1.0$ in panel (f) for 3D systems.

small relative to the separation between sites.

The interpretation from the $D = 1$ participation ratio distributions that all wave functions are localized is in a sense not surprising. With the theoretical framework of Anderson localization having been introduced more than 50 years ago²⁹, a significant body of work (both in experiment and theoretical calculations) has examined the tendency for random potentials to localize electronic states very effectively in one dimensional systems, even for weak random potentials. Moreover, the availability of cold atom traps with coherent quantum states where the underlying one dimensional potential may be tailored in a variety of ways has made possible the study of localization properties of 1D systems in a controlled manner. In this vein, a direct experimental observation of localization has recently been achieved in a Bose-Einstein condensate with the random (diagonal) potential set up by a laser speckle³⁰ with results in accord with theoretical descriptions³¹. Bichromatic aperiodic potentials are not purely random uncorrelated disorder, but nonetheless have been found in experiment and theoretical analysis^{32–34} to be very effective in localizing quantum states. In this work, we show using finite size scaling analysis that off-diagonal disorder inherent in one dimensional amorphous systems leads to the localiza-

tion of all electronic states in the absence of random site potentials.

For $D = 2$, the evolution of the participation ratio with increasing L depends on the hopping integral decay length l . IPR histograms for various γ values are shown in the six panels of Fig. 4; as in the 1D case, successive values of L differ by a factor of 2, and participation ratio distributions for $L = \{5, 10, 20, 40, 80\}$ appear together on the same graph. For short hopping ranges $l = \gamma^{-1}$, there are maxima in the high IPR regime which subsume a large share of the total statistical weight; apart from small vacillations, the distributions have a unimodal envelope, as seen in IPR histograms calculated for one dimensional systems. Moreover, the convergence of histograms with respect to L is an indication of the localization of all states in the thermodynamic limit.

For longer decay lengths l (i.e. for $\gamma \leq 1.5$) participation ratio distributions obtained for 2D amorphous systems lack the unimodal sharply peaked structure seen for small l and unlike the $l \ll 1$ counterparts, seem not to converge with respect to increases in L . Instead, histograms become bimodal as statistical weight is transferred to the left, toward the lower IPR regime.

The migration of statistical weight toward lower IPR values and more extended character, is indicative of the possible existence of extended states, and the effect is particularly striking for the smallest decay rates $\gamma = 0.75$ and $\gamma = 0.5$. The systematic transfer with increasing L of probability density to smaller IPR values is manifest as a steady leftward shift of the trailing (low IPR) edge and of the histogram with the nearby maximum also born leftward. In fact, the shift both of the peak and the leftmost front is constant in magnitude each time the system size L is doubled; since the abscissa is $\log_{10}(\text{IPR})$, the latter trend corresponds to a power law scaling $L^{-\beta}$ for the left trailing edge and low IPR peak.

Participation ratio histograms for 3D systems are displayed in Fig. 5. As in the large l limit for 2D systems, a portion of the participation ratio statistical weight shifts systematically to lower IPR values. The size of the emerging peak and the amount of probability density which migrates leftward increases with l , even as the cusp-shaped maximum in the low IPR regime decreases in amplitude and overall statistical weight.

A noteworthy feature for $l \leq 1$ is the robustness of the probability density contained in the leftward shifting peak. That the packet moves systematically toward lower IPR values without leaving behind any statistical weight is compatible with the existence of a finite fraction of extended states in the bulk limit. Thus, for 3D amorphous systems, there is a dichotomy in the way the distribution changes, where the leftward shifting probability density corresponding to extended wave functions contrasts with the localized states encompassed in the high IPR region of the histogram, which ceases to evolve with increasing L . With increasing tunneling matrix element range l , the balance shifts in favor of the extended states as more and more statistical weight is swept into

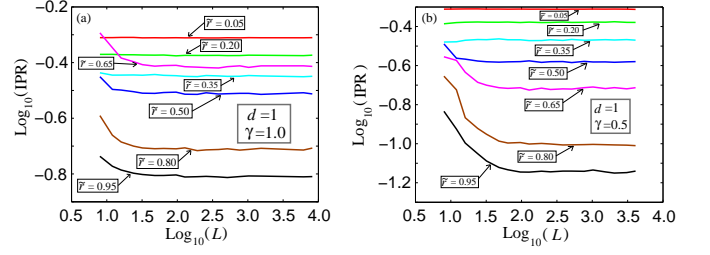


FIG. 6: (Color Online) Log-Log graphs of channel averaged IPR versus L for 1D systems in the case of a 100 channel scheme. Panel (a) and panel (b) correspond to hopping integral decay rates $\gamma = 1.0$ and $\gamma = 0.5$ respectively.

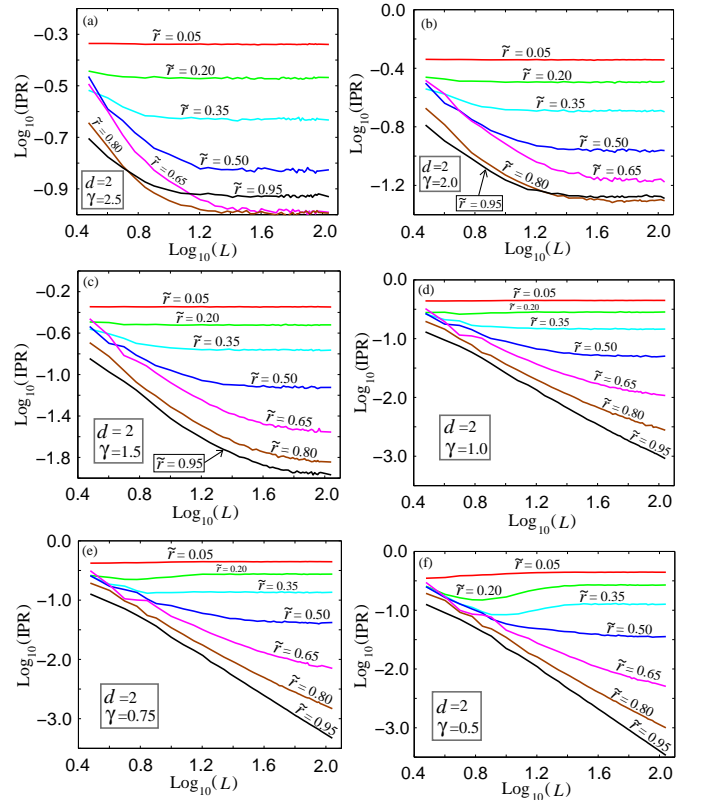


FIG. 7: (Color Online) Log-Log graphs of channel averaged IPR versus L for 2D systems in the case of a 100 channel scheme with hopping integral decay rates ranging from $\gamma = 2.5$ in panel (a) to $\gamma = 0.5$ in panel (f).

the peak moving toward lower IPR values. Nonetheless, as embodied in the part of the distribution which does not change with increasing L , a finite fraction of the wave functions are localized even for very small values of the decay rate γ .

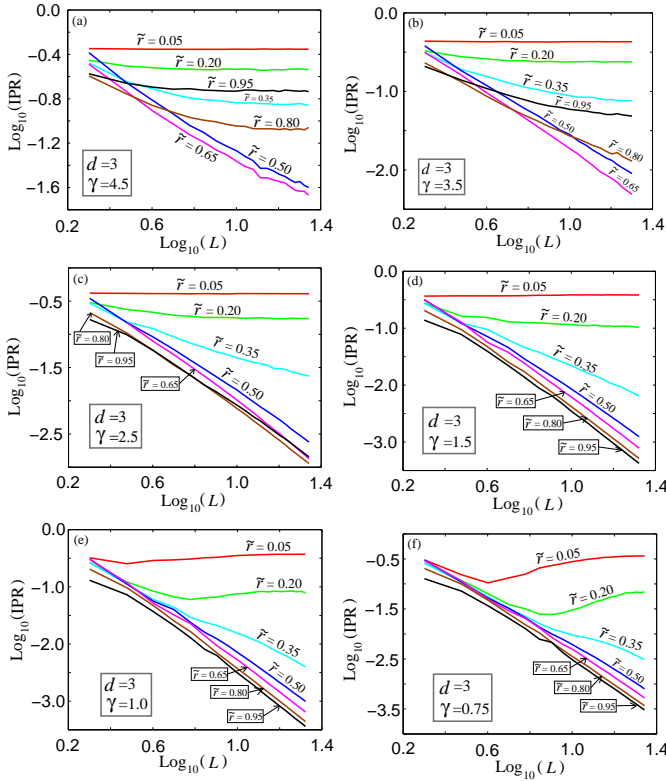


FIG. 8: (Color Online) Log-Log graphs of channel averaged IPR versus L for 3D systems in the case of a 100 channel scheme with hopping integral decay rates ranging from $\gamma = 4.5$ in panel (a) to $\gamma = 0.75$ in panel (f).

IV. THE CHANNEL AVERAGED PARTICIPATION RATIO

With long-range positional order absent in the amorphous systems we examine, the eigenstate energy is the only good quantum number available, and in this work we show that the energy eigenvalue is a unique determinant as to whether electronic states are either extended or localized for a particular energy with the simultaneous presence of localized and extended states ruled out as a possibility.

Determining if a wave function ψ is localized or extended entails calculating participation ratio statistics for many L values and using finite size scaling to access the $L \rightarrow \infty$ limit, with a vanishing IPR in the bulk limit a hallmark of extended states. The random character of the disorder precludes the study of the evolution of individual states with increasing system size, and instead we must analyze aggregates of wave functions across a range of system sizes. Electronic states are parameterized by energy eigenvalues, and one possible choice is to partition the states into channels centered about uniformly spaced energies E' which encompass an energy interval δE narrow enough to capture information specific to wave functions with energies very close to E' , but broad enough to suppress statistical fluctuations.

The DOS statistical distributions shown in Fig. 2 are sharply peaked, with a rapid decrease in the probability density away from the maximum. In a practical sense, the DOS heterogeneity poses a challenge for a scheme where the global energy range ΔE between the ground state energy E_{\min} and the highest excited state energy E_{\max} is partitioned into small intervals δE of uniform size; statistical fluctuations will plague channels far from the DOS maximum where the statistical weight for eigenstates is sharply reduced.

In lieu of energy, to circumvent the problem of non-uniform statistics, states are labeled with the normalized energy eigenvalue rank \tilde{r} . For finite systems, the rank number is assigned by calculating energy eigenvalues and corresponding wave functions for a large number of configurations of disorder. The normalized rank number is $\tilde{r} \equiv r/N$ where N is the total number of states and r is the global eigenvalue rank within the large aggregate. We find $n = 100$ yields channel widths $\delta\tilde{r}$ sufficiently narrow for channel averages to be representative of the normalized rank \tilde{r} at the center of the channel, yet broad enough to provide sufficient statistics for analysis; a parallel calculation for $n = 50$ yields results in quantitative agreement with the $n = 100$ scheme, direct verification that $n = 100$ is large enough to avoid systematic admixture effects from the finite channel width $\delta\tilde{r}$.

Channel averaged IPR results appear in Fig. 6, Fig. 7, and Fig. 8 for 1D, 2D, and 3D systems, where the horizontal axis is $\log_{10}(L)$ for each case. The participation ratio results for the one dimensional systems are in a sense most readily interpreted. IPR curves initially decrease for small system sizes, but quickly level out and approach asymptotically finite values even for the small decay constant $\gamma = 0.5$. The latter phenomenon is consistent with the convergence of the global IPR probability distribution with increasing L , interpreted as a sign that all wave functions are localized in one dimensional systems irrespective of the hopping decay parameter γ .

For $D = 2$, there is a bifurcation in the way the IPR channel averages vary with increasing L with the precise behavior determined by the hopping range $l = \gamma^{-1}$. For large γ (i.e. especially for $\gamma = 2.0$ and $\gamma = 2.5$), the IPR traces level out and approach finite asymptotic bulk values corresponding to localized states, much as occurs for 1D amorphous systems. On the other hand, in the case of smaller γ , where there is a greater likelihood that states with extended character are supported, it is not definitively conclusive that the participation ratio curves approach asymptotically finite values for very large system sizes. Broadly speaking, for $D = 2$ IPR traces are most likely to level out and tend to a finite value for smaller \tilde{r} , or for energies near the ground state. For $\gamma \leq 1.0$, there are channel average curves which in principal may keep a finite negative slope as $L \rightarrow \infty$, which on a logarithmic scale is tantamount to a vanishing IPR in the thermodynamic limit.

Notwithstanding the persistently downward slope, an unambiguous determination that the monotonically de-

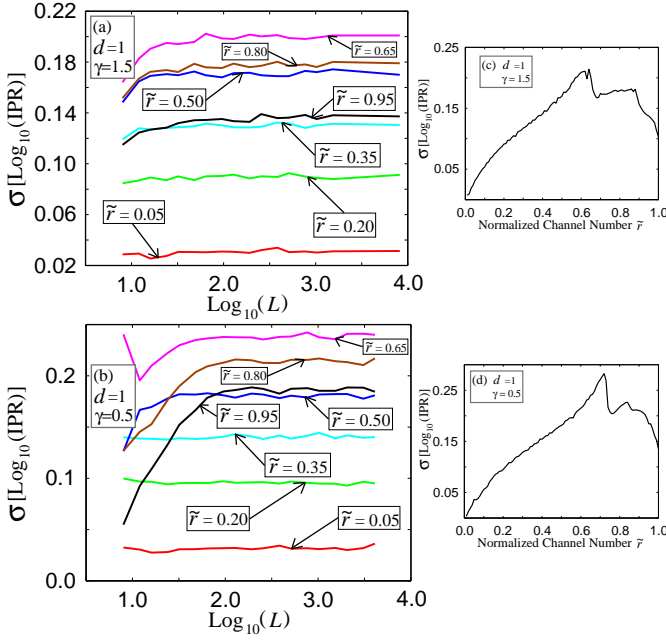


FIG. 9: (Color Online) Intra-channel standard deviations of $\log_{10}(\text{IPR})$ plotted for the $D = 1$ case. Graphs in panels (a) and (c) correspond to relatively large $\gamma = 1.5$, while plots in panels (b) and (d) are calculated for a more gradual hopping integral decay, $\gamma = 0.5$. Graphs on the left show σ versus $\log_{10}(L)$ for various normalized channel numbers \tilde{r} , while the rightmost panels are plots of $\sigma[\log_{10}(\text{IPR})]$ with respect to the rank \tilde{r} for large L .

creasing channel averages represent extended states is hampered by the upward concavity in most of the IPR curves, where except for the very highest \tilde{r} (i.e. for $\tilde{r} = 0.95$ where the concavity appears to be neutral), there is a progressive reduction in the magnitude of the downward slope which could eventually cause the channel averaged participation ratio to level out at a finite value. To determine in a rigorous way if the participation ratios vanish for $L \rightarrow \infty$ or instead approach a finite value, a finite size scaling analysis, described in Section V, is needed.

As in the case of the 2D systems, for $D = 3$, there are in a broad sense two ways in which IPR curves scale with L . For very large decay rates (e.g. $\gamma = 4.5$), the participation ratio channel averages seem to level out and tend to finite values. On the other hand for smaller γ , instead of the upward concavity seen in the case of two dimensional systems, many of the curves are concave downward with the rate of decrease of the channel averages increasing with L . With the downward slope becoming greater instead of showing signs of faltering as in $D = 2$, it is possible to conclude without further analysis that the participation ratio tends to zero in the bulk limit.

With channel averages only providing the mean participation ratio, it is important to be certain the IPR values obtained in this manner represent the characteristics of all of the states encompassed in a channel. The most

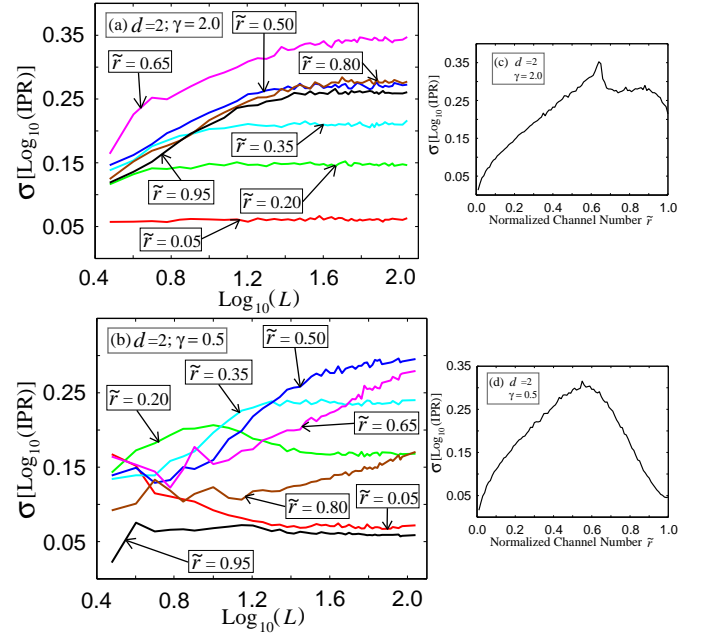


FIG. 10: (Color Online) Intra-channel standard deviations of $\log_{10}(\text{IPR})$ plotted for the $D = 2$ case. Graphs in panels (a) and (c) correspond to relatively large $\gamma = 2.0$, while plots in panels (b) and (d) are calculated for a more gradual hopping integral decay, $\gamma = 0.5$. Graphs on the left show σ versus $\log_{10}(L)$ for various normalized channel numbers \tilde{r} , while the rightmost panels are plots of $\sigma[\log_{10}(\text{IPR})]$ with respect to the rank \tilde{r} for large L .

vital task in this vein is to rule out the possibility of the coexistence of localized and extended states for a specific channel index \tilde{r} (or energy E). To tackle this question, we calculate the standard deviation σ of $\log_{10}(\text{IPR})$ across a channel with results appearing Fig. 9 for $D = 1$, Fig. 10 for $D = 2$, and Fig. 11 for $D = 3$. With increasing L , the quantity $\sigma[\log_{10}(\text{IPR})]$ will either diverge or tend to a finite value. While a divergence indicates a dual presence of extended and localized states (coexistence), a standard deviation of participation ratio logarithms which tends to a finite value for $L \rightarrow \infty$ is an indication that there are either localized or extended wave functions, but not both (exclusivity).

If only localized states are present, the the standard deviation will converge to a limiting value (σ is in general finite even in the thermodynamic limit since some wave functions are more spread out than others due to disorder fluctuations) and become a bulk characteristic when $L \gg \xi$, where ξ is the largest decay length scale of the broadest states. On the other hand, for a suite of purely extended states, the IPR for each wave function will tend to zero with a concomitant divergence of $\log_{10}(\text{IPR})$. Although the magnitude of the ensemble average $\langle \log_{10}(\text{IPR}) \rangle$, which is negative in sign, grows without bound for increasing L for a rank \tilde{r} or energy E supporting extended states, it is nevertheless not clear that σ diverges since the standard deviation measures the

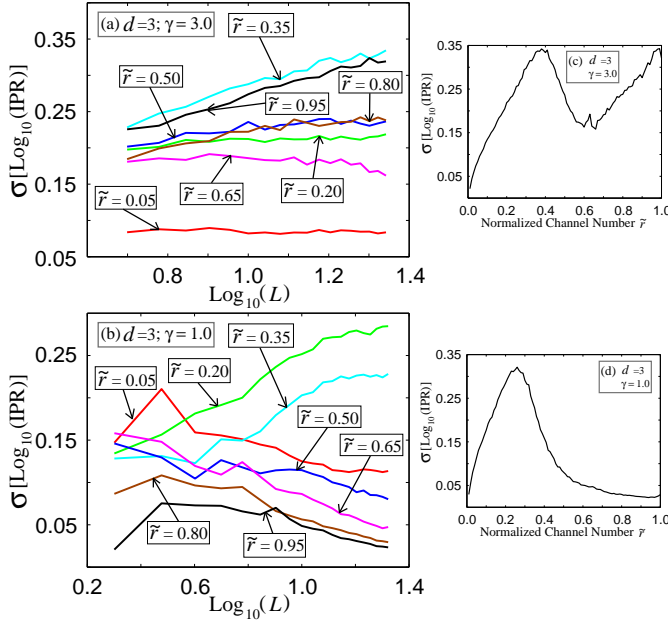


FIG. 11: (Color Online) Intra-channel standard deviations of $\log_{10}(\text{IPR})$ plotted for the $D = 3$ case. Graphs in panels (a) and (c) correspond to relatively large $\gamma = 3.0$, while plots in panels (b) and (d) are calculated for a more gradual hopping integral decay, $\gamma = 1.0$. Graphs on the left show σ versus $\log_{10}(L)$ for various normalized channel numbers \tilde{r} , while the rightmost panels are plots of $\sigma[\log_{10}(\text{IPR})]$ with respect to the rank \tilde{r} for large L .

spread in the participation ratios, not their magnitude. In the global IPR histograms shown in Fig. 4 and Fig. 5 for $D = 2$ and $D = 3$, the fact that packets of probability density which migrate lower $\log_{10}(\text{IPR})$ with increasing L tend to maintain their shape and profile even as the participation ratio decreases by several orders of magnitude suggests σ may remain finite even as the average $\langle \log_{10}(\text{IPR}) \rangle$ diverges.

In the coexistence scenario, with a simultaneous presence of extended and localized wave functions, there will be a divergence in $\sigma[\log_{10}(\text{IPR})]$ since the packet of probability density for localized states remains fixed with increasing L while the peak corresponding to states with extended character is conveyed toward more negative $\log_{10}(\text{IPR})$. Since the standard deviation provides a measure of the increasing separation of the two peaks, $\sigma[\log_{10}(\text{IPR})]$ must diverge as $L \rightarrow \infty$ if localized and extended electronic states are present for the same energy E or rank \tilde{r} .

To determine if for any combination of system parameters σ converges to a finite value (exclusivity) or diverges (coexistence), we plot $\sigma[\log_{10}(\text{IPR})]$ versus $\log_{10}(L)$ in the left panels of the graphs in Figs. 9 Figs. 10, and Figs. 11. In addition, the right panels show σ with respect to \tilde{r} for large L to provide a glimpse of $\sigma[\log_{10}(\text{IPR})]$ for large L . The σ curves for the cases $D = 1$, and $D = 2$, and $D = 3$ are concave downward in the large L regime, and seem to level out and tend

to finite values. In addition, for the largest system size considered in this work and plotted in the right panels of Fig. 9, Fig. 10, and Fig. 11, $\sigma[\log_{10}(\text{IPR})]$ are low in magnitude, and do not exceed $\sigma[\log_{10}(\text{IPR})] = 0.35$ for which the spread of the participation ratios is at most a factor of two.

V. PARTICIPATION RATIOS IN THE THERMODYNAMIC LIMIT

The primary aim in the finite size scaling analysis is to calculate IPR_0 , the channel averaged participation ratio in the thermodynamic limit. For the IPR dependence for moderate to large L , we use a power law formula, $\text{IPR}(L) = \text{IPR}_0 + \alpha_1 L^{-\beta} + \alpha_2 L^{-\delta}$ where IPR_0 is the participation ratio in the bulk limit, β is the leading order scaling exponent, and δ is the exponent for the next to leading order contribution to scaling; α_1 and α_2 are amplitudes. We obtain the parameters IPR_0 , β , δ , α_1 , and α_2 in a nonlinear least squares calculation by minimizing the sum of the square of the relative differences $\Delta_{\text{LSF}} \equiv \frac{1}{m} [\sum_{i=1}^m (\frac{\text{IPR}^{\text{CA}}(L_i) - \text{IPR}^{\text{LSF}}(L_i)}{\text{IPR}^{\text{CA}}(L_i)})^2]^{1/2}$ (i.e. with L_1 and L_m the smallest and largest systems examined, respectively) of the data gleaned from the IPR channel averages $\text{IPR}^{\text{CA}}(L)$ and the theoretical scaling expression $\text{IPR}^{\text{LSF}}(L)$. To find the optimal fit, we use a stochastic algorithm with the quantity Δ_{LSF} treated as an “energy” to be minimized by randomly perturbing IPR_0 , amplitudes α_1 and α_2 , and exponents β and δ . Only Monte Carlo moves which decrease Δ_{LSF} (and hence incrementally improve the fit) are accepted, and the IPR(L) parameters are suitably converged after 4×10^5 attempts to shift the five unknown parameters in IPR(L) in a stochastic fashion.

Participation ratios extrapolated to the bulk limit are displayed for $D = 1$, $D = 2$, and $D = 3$ in Fig. 12. The main graphs are calculated for 100 channel partitions, whereas the insets show results for a 50 channel scheme. The good agreement among the 100 and 50 channel bulk IPR values indicates convergence of the bulk IPR values with respect to the number of channels.

Bulk limit Participation ratios for 1D systems are plotted in panel (a) of Fig. 12. Notwithstanding a nonmonotonic variation of IPR in the normalized channel number \tilde{r} the $D = 1$ results are finite in all cases, dipping only slightly below $\text{IPR}_0 = 0.1$ even for hopping integral decay rates as low as $\gamma = 0.5$, and thus are indicative of localization of all wave functions irrespective of the size of the hopping range l .

Extrapolated IPR results for $D = 2$ shown in panel (b) of Fig. 12 are non-monotonic, generally decreasing precipitously near $\tilde{r} = 0$ and ultimately recovering in the vicinity of $\tilde{r} = 1$. With increasing l , the participation ratio trough becomes broader and deeper, while the recovery to higher IPR values is muted. Eventually, for $\gamma \leq 1$, the minimum reaches the horizontal axis, where

$\text{IPR}_0 = 0$, and there is no return to higher participation ratios near $\tilde{r} = 1$; hence the \tilde{r} axis is effectively divided into two regions where wave functions are localized below a threshold \tilde{r}_c and extended above it.

The $D = 3$ bulk IPR curves in panel (c) of Fig. 12 differ in significant ways from the corresponding participation ratios calculated either for 1D or 2D systems. In general, looking from $\tilde{r} = 0$ to $\tilde{r} = 1$, the bulk IPR initially makes a sharp descent until intersecting the horizontal axis. The slope downward decreases with the hopping range l , and the normalized channel number where the bulk IPR becomes zero retreats to smaller \tilde{r} with increasing scale l . For $\gamma \leq 1$, there is only a single mobility boundary; the IPR falls to zero, coincides with the abscissa, and does not climb again to finite values.

On the other hand, although for larger γ the extrapolated participation ratio curves initially descend as in $\gamma \leq 1$ and eventually become zero, in the upper \tilde{r} range, the IPR begins to increase and is again finite. Thus, for $\gamma > 1$, two mobility boundaries separate an intermediate range of energies where the participation ratio vanishes (corresponding to extended states) from energy regimes where wave functions are localized. The width of the interval where the $\text{IPR}_0 = 0$ constricts width increasing γ , though even for quite large values of the decay constant (i.e. for $\gamma = 5.5$), the extrapolated IPR seems at least to briefly touch the horizontal axis before rising again to finite values with a locally “v” shaped profile. Participation ratio curves corresponding to smaller γ values have broader minima, but also have local symmetry about the same point in the vicinity of $\tilde{r} = 0.58$.

We use bulk participation ratios to construct phase diagrams for the tight binding wave functions; for the 1D case, there is only a single phase with the electronic states are localized in all cases, while phase portraits for $D = 2$ (shown in Fig. 13 and Fig. 14) and $D = 3$ (displayed in Fig. 15 and Fig. 16) show areas of extended states and phases in which all of the wave functions are localized. For the 2D case, the wedge of extended states, broadest for $\gamma = 0.5$, tapers with increasing γ and vanishes altogether in the vicinity of $\gamma = 1.5$, as indicated by the broken lines which are extrapolations.

For $D = 3$, the swath of extended states is quite broad for $\gamma \sim 1.0$, encompassing most of the eigenstates and the associated range of eigenstates energies. As in the 2D case, a smaller portion of the wave functions are extended with increasing γ . for moderate to large hopping integral decay lengths (i.e. for $\gamma \geq 3.0$), the band of extended states rapidly constricts with the extended phases asymptotically symmetric about $\tilde{r} = 0.58$. Fig. 16 is the phase diagram with the vertical axis rendered in terms of energies instead of normalized rank \tilde{r} . Again, the interval of extended states becomes sharply narrower with increasing γ .

Although the extended state phase persists for large values of γ (i.e. even for $\gamma > 5.0$), the decrease of the width is very rapid, and we examine the possibility that the decrease may be exponential in the hopping integral

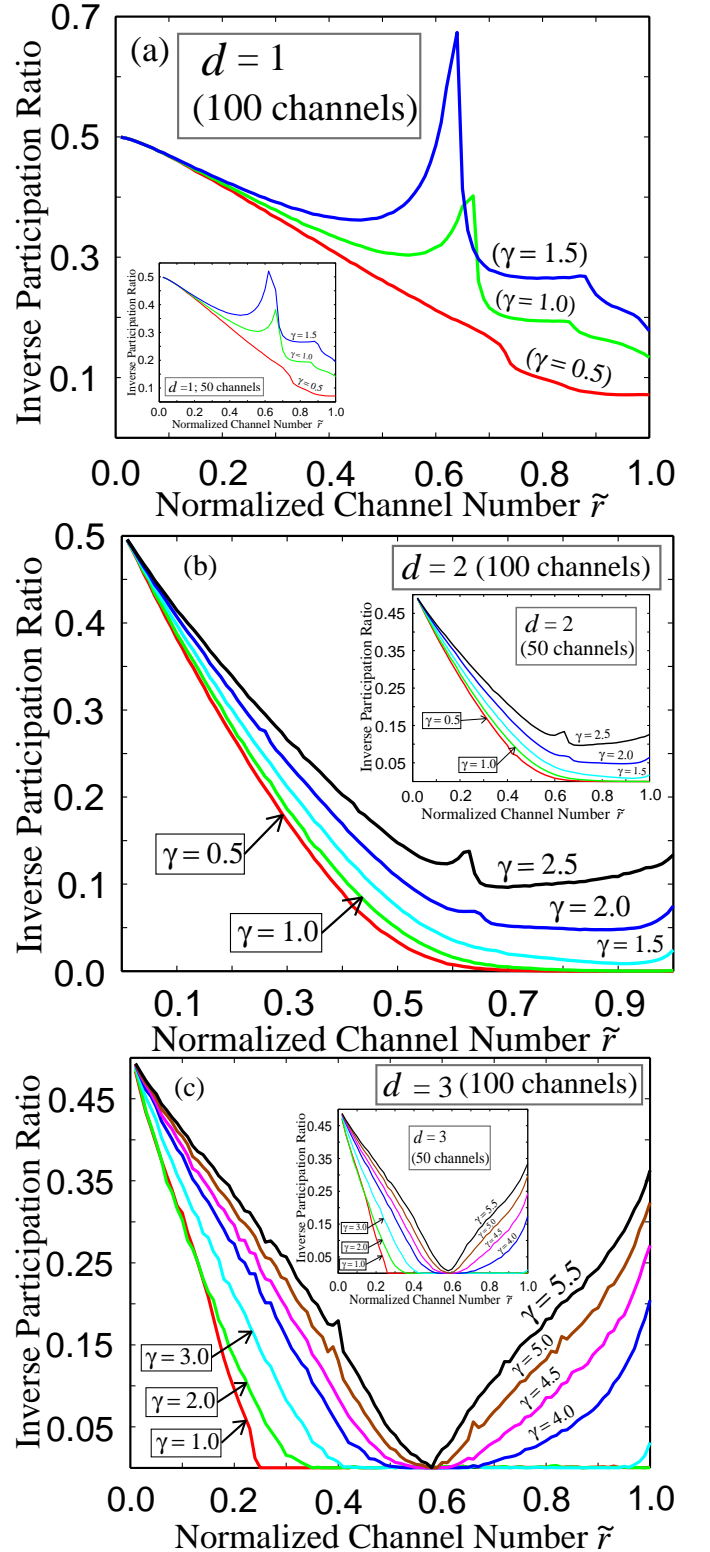


FIG. 12: (Color Online) Inverse Participation Ratio profiles graphed for strong decay rates γ [ranging from $\gamma = 3.5$ in panel (a) to $\gamma = 2.0$ in panel (d)] for 1D systems.

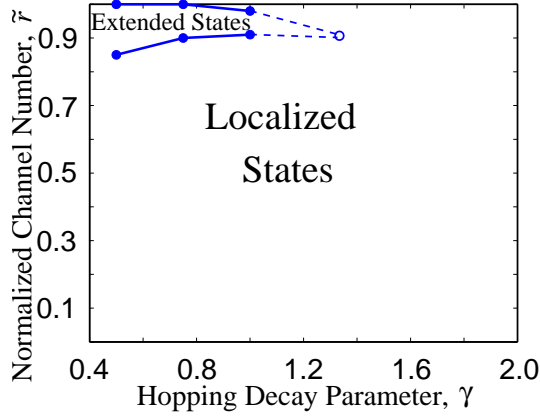


FIG. 13: (Color Online) Phase portrait for 2D systems with the hopping decay parameter γ on the abscissa and the channel number \tilde{r} on the vertical axis. The broken lines are extrapolated parts of the phase boundary.

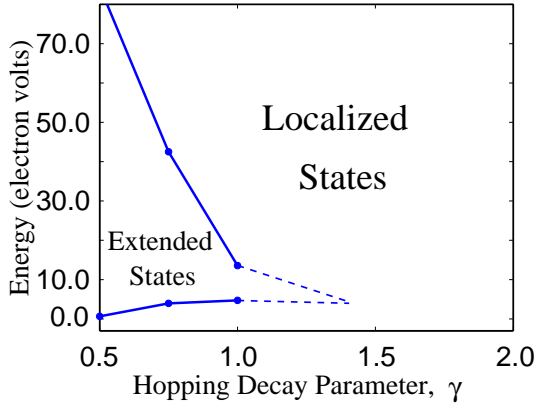


FIG. 14: (Color Online) Phase diagram for the $D = 2$ case with the hopping decay parameter γ on the abscissa and the eigenstate energy (in electron volts) on the vertical axis. The broken lines indicates extrapolated parts of the phase boundary.

decay rate γ . Fig. 17 displays a graph of base ten logarithm of the width of the phase where eigenstates are extended; the main plot shows $\log_{10}[w(\tilde{r})]$ with respect to γ , while the inset is a plot of $\log_{10}[w(E)]$ versus γ . The asymptotically linear dependence of the logarithm of w , which is seen whether one considers the the width $w(E)$ of the energy interval or $w(\tilde{r})$ of the normalized rank, is consistent with an exponential dependence $w \propto e^{-A\gamma}$ for moderate to large γ .

VI. CONCLUSIONS AND FUTURE WORK

We have calculated the energy Density of States and, using the Inverse Participation Ratio, we have examined the characteristics of electronic states in amorphous systems in one, two, and three dimensions for hopping matrix elements which decay exponentially in the separation

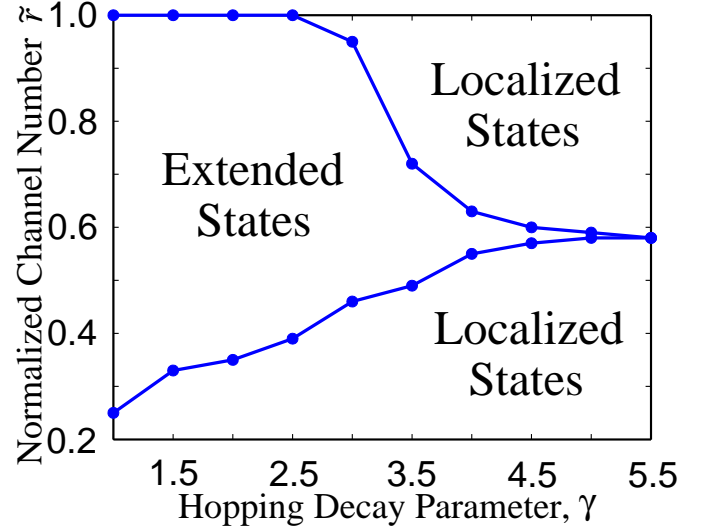


FIG. 15: (Color Online) Phase portrait for 3D systems with the hopping decay parameter γ on the abscissa and the channel number \tilde{r} on the vertical axis.

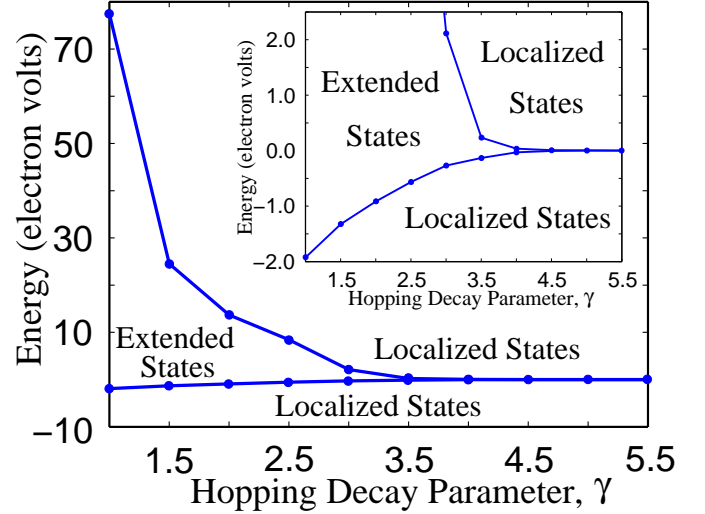


FIG. 16: (Color Online) Phase diagram for the $D = 3$ case with the hopping decay parameter γ on the abscissa and the eigenstate energy (in electron volts) on the vertical axis. The graph inset is a closer view of the bifurcation region.

distance between neighboring sites in the context of a tight binding model. We have calculated global IPR statistical distributions, which have a rich multimodal structure for systems in two and three dimensions in contrast to the simple sharply peaked profiles consistently seen for $D = 1$.

Partitioning wave functions according to the normalized eigenvalue rank \tilde{r} has yielded channel averaged participation ratios, which we have shown to be representative of wave functions for a specific energy E or normalized rank \tilde{r} . By applying finite size scaling to each of the channel averages, we have obtained participation

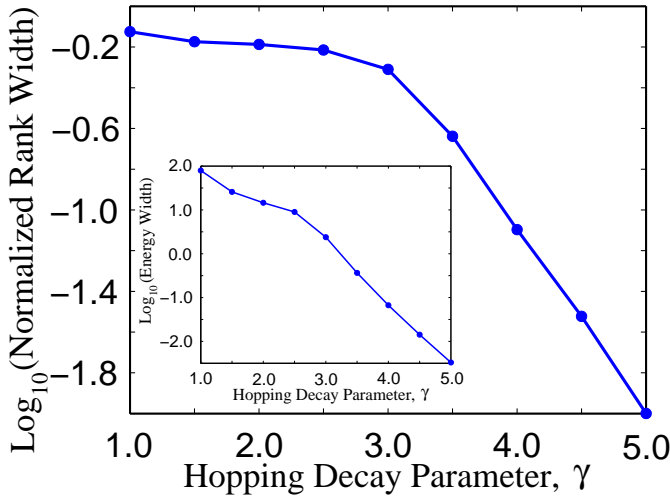


FIG. 17: (Color Online) Logarithm of the width of the extended state region plotted versus the decay parameter γ . The main graph shows the normalized rank width $w(\tilde{r})$, and the inset plot displays the width of the corresponding energy interval $w(E)$.

ratios in the thermodynamic limit; using the latter, we have constructed phase portraits of the eigenstates with respect to localization.

In 1D, wave functions are strongly localized in all cases, whereas results for 2D indicate the presence of a critical decay parameter γ_c , with localization for $\gamma > \gamma_c$ and existence of extended states below γ_c . In the 3D case, extended states also are admitted, and the wave functions with extended character occur even for quite large γ values, although the interval of energies supporting extended states diminishes with γ , asymptotically scaling as $e^{-A\gamma}$ with increasing γ . The swath of extended states is flanked by regions where wave functions are localized, with the two interfaces interpreted as mobility bound-

aries.

In future studies, disorder schemes will be considered in which the severity of the disorder is tuned from mild to quite strong by perturbing a regular periodic crystal lattice and introducing random perturbations δ in the positions of the hopping sites. The disordering shifts δ may be introduced, e.g., from a Gaussian distribution with a RMS magnitude σ . Among the salient germane questions to be investigated in this manner is whether there is a threshold in typical displacement magnitudes where extended states may survive in $D = 1$ and $D = 2$ if random displacements in atomic positions are sufficiently small in relation to the crystal lattice constant. Given the fragility of extended character in $D = 1$, one might predict that even a small random perturbation in the site positions from a periodic configuration might induce localization in a one dimensional lattice. On the other hand, in two dimensions it may be that there is a perturbation level beyond which the disordering influence causes most or all of the states to be localized, with predominantly extended character below the perturbation threshold.

In the present study, we have concentrated on short-range couplings, as might be appropriate in an exchange type coupling scheme. Nonetheless, it would be useful also to examine a power law decay to see if the severity of localization effects are reduced in one dimension, and if *bona fide* extended states exist under these conditions.

Acknowledgments

Useful discussions with Euyheon Hwang, John Biddle, Bin Wang, and Sankar Das Sarma are gratefully acknowledged. The numerical analysis has been facilitated by use of the 360 node, 2700 CPU University of Maryland, College Park HPCC parallel computing cluster.

-
- ¹ F. Bloch, Z. Physik **52**, 555 (1928).
 - ² J. M. Ziman, *Models of Disorder: The Theoretical Physics of Homogeneously Disordered Systems*, Cambridge University Press, P. 472, (1979).
 - ³ F. Hensel, W.W. Warren, *Fluid Metals*, Princeton University Press (1999).
 - ⁴ A. Blumen, J. P. Lemaistre, and I. Mathlouthi, J. Chem. Phys. **81**, 4610 (1984).
 - ⁵ W. Y. Ching and D. L. Huber, Phys. Rev. B **25**, 1096 (1982).
 - ⁶ D. E. Logan and M. D. Winn, J. Phys. C **21**, 5773 (1988).
 - ⁷ M. D. Winn and D. E. Logan, J. Phys.: Condens. Matter **1**, 1753 (1989).
 - ⁸ I. J. Bush, D. E. Logan, P. A. Madden, and M. D. Winn, J. Phys.: Condens. Matter **1**, 2551 (1989).
 - ⁹ J. Brndiar and P. Markoš, Phys. Rev. B, **77**, 115131 (2008).
 - ¹⁰ A. Wobst, G.-L. Ingold, P. Hänggi, and D. Weinmann, Phys. Rev. B **68**, 085103 (2003).
 - ¹¹ A. Mildenberger, F. Evers, and A. D. Mirlin, Phys. Rev. B **66**, 033109 (2002).
 - ¹² J. Bauer, T.-M. Chang, and J. L. Skinner, Phys. Rev. B **42**, 8121 (1990).
 - ¹³ M. Schreiber, Phys. Rev. B **31**, 6146 (R), (1985).
 - ¹⁴ F. J. Dyson, Phys. Rev. **92**, 1331 (1953).
 - ¹⁵ R. Gade, Nucl. Phys. B **398**, 499 (1993).
 - ¹⁶ D. A. Parshin and H. R. Schober, Phys. Rev. B **57**, 10232 (1998).
 - ¹⁷ V. Z. Cerovski, Phys. Rev. B **62**, 12775 (2000).
 - ¹⁸ K. Takahashi and S. Iida, Phys. Rev. B **63**, 214201 (2001).
 - ¹⁹ S.-J. Xiong and S. N. Evangelou, Phys. Rev. B **64**, 113107 (2001).
 - ²⁰ A. M. García-García and E. Cuevas, Phys. Rev. B **74**, 113101 (2006).
 - ²¹ M. K. Gibbons, D. E. Logan, and P. A. Madden, Phys. Rev. B **38**, 7292-7302 (1988).
 - ²² B. Cai and D. A. Drabold, Phys. Rev. B **79**, 195204 (2009).

- ²³ M. Turek, J. Siewert, and J. Fabian, Phys. Rev. B **78**, 085211 (2008).
- ²⁴ Sébastien Blaineau and Philippe Jund, Phys. Rev. B **70**, 184210 (2004).
- ²⁵ J. M. Holender and G. J. Morgan, Modelling Simul. Mater. Sci. Eng. **2**, 1-8 (1994).
- ²⁶ Th. Kosłowski and W. Von Niessen, J. Phys. Condens. Matter **4**, 6109 (1992).
- ²⁷ R. Atta-Fynn, P. Biswas, P. Ordejón, and D. A. Drabold, Phys. Rev. B **69**, 085207 (2004).
- ²⁸ N. Metropolis, A. W. Rosenbluth, M. N. Rosenbluth, A. H. Teller, and E. Teller, J. Chem. Phys., **21**, 1087, (1953).
- ²⁹ P. W. Anderson, Phys. Rev. **109**, 1492 (1958).
- ³⁰ J. Billy, V. Josse, Z. Zuo, A. Bernard, B. Hambrecht, P. Lugan, D. Clément, L. Sanchez-Palencia, P. Bouyer, and A. Aspect, Nature **453**, 891-894 (2008).
- ³¹ E. Gurevich and O. Kenneth, Phys. Rev. A **79**, 063617 (2009).
- ³² J. Biddle, B. Wang, D. J. Priour, Jr., and S. Das Sarma, Phys. Rev. A **80**, 021603(R) (2009).
- ³³ J. Biddle and S. Das Sarma, Phys. Rev. Lett. **104**, 070601 (2010).
- ³⁴ J. Biddle, D. J. Priour, Jr., B. Wang, and S. Das Sarma, Phys. Rev. B **83**, 075105 (2011).